# Quantum Confinement in Si and Ge Nanostructures

E.G. Barbagiovanni,[1,*] D.J. Lockwood,[2] P.J. Simpson,[1] and L.V. Goncharova[1]

[1] *Department of Physics and Astronomy, The University of Western Ontario, London, Ontario, Canada, N6A 3K7*
[2] *National Research Council Ottawa, Ontario, Canada, K1A 0R6*

(Dated: May 19, 2011)

We use perturbative effective mass theory as a toy theoretical model for quantum confinement (QC) in Si and Ge quantum wells (QWs), wires (Q-wires) and dots (QDs). Within the limits of strong, medium, and weak QC, valence and conduction band edge energy levels (VBM and CBM) were calculated as a function of QD diameters, QW thicknesses and Q-wire diameters. Crystalline and amorphous quantum systems were considered separately. Calculated band edge levels with strong, medium and weak QC models were compared with experimental VBM and CBM reported from X-ray photoemission spectroscopy (XPS), X-ray absorption spectroscopy (XAS) or photoluminescence (PL). Experimentally, the dimensions of the nanostructures were determined directly, by transmission electron microscopy (TEM), or indirectly, by x-ray diffraction (XRD), or by XPS. We found that crystalline materials are best described by a medium confinement model, while amorphous materials exhibit strong confinement regardless of the confinement dimensions of the system. Our results indicate that spatial delocalization of the hole in amorphous versus crystalline nanostructures is the important parameter determining the magnitude of the band gap expansion, or the strength of the quantum confinement. In addition, the effective masses of the electron and hole are discussed as a function of crystallinity and spatial confinement.

PACS numbers: 73.21.-b,73.22.-f,78.67.-n,61.46.-w,81.07.-b

## I. INTRODUCTION

The phenomenon of quantum confinement (QC) is defined as the modification in the free particle dispersion relation as a function of a system's spatial dimension. Quantum mechanics predicts that if a free electron is confined within a potential barrier, such that the spatial dimension of the wave amplitude of the electron is greater than or equal to the spatial dimension of the potential barrier, then the energy levels of the electron become discrete. Furthermore, the electron energy levels are inversely proportional to the size of the system. Therefore, QC is observed in optical experiments when the dimension of the system is systematically reduced and an increase in the absorbed/emitted photon energy is measured corresponding to electron transitional states.

For semiconductor materials the essential features of QC are directly carried over from the single electron model. The optical transitional energies refer to the transition between the valence band maximum (VBM), considered as the ground state energy, and the conduction band minimum (CBM), the first excited state. As a result, the emitted photon energy is directly proportional to the gap energy ($E_G$). The confinement potential is determined by the alignment of the respective Fermi levels when a material of a $E_{G1}$ is surrounded by a material of a $E_{G2}$, with $E_{G1} < E_{G2}$.[1] Therefore, QC in a semiconductor material implies the energy levels in the conduction band (CB) and the valence band (VB) become discrete. In addition, QC increases the oscillator strength in a semiconductor nanostructure compared to the bulk state, making materials like Si viable for optoelectronics.[2]

Semiconductor materials contain holes that can dramatically change the energy of the emitted photon. Using time-reversal symmetry, it can be shown that the hole has all the properties of an ordinary particle.[3] However, electrons and holes have different effective masses due to their respective positions in the Brilloun zone, leading to different interaction strengths with the crystal field. If direct electron-hole (e-h) recombination occurs across the band gap, the energy of the resulting photon is the kinetic energy of the electron plus the hole, which is a function of the effective mass subject to the boundary conditions of the material. Furthermore, the electron and hole can form a hydrogenic or positronium-like exciton, a bound state of the constituent particles, thus modifying the photon energy during the recombination event by the Coulomb interaction between the electron and hole. Therefore, it is important to understand the kinetics of the hole and the effective mass of the e-h pair.

Beyond direct e-h recombination, other factors, given below, affect the electronic dispersion and/or the PL dynamics, frequently observed as a stretched exponential decay behaviour.[4] This list is not meant to be exhaustive; nanostructures have been shown to exhibit higher order effects.[5] For a review of these factors and general properties of low-dimensional structures, see Refs. 5–7.

- Surrounding matrix: A nanostructure surrounded by a matrix with a different dielectric constant changes the strength of interaction with the image charges in that matrix.[7] In addition, the choice of the matrix material can indirectly effect all of the subsequent factors considered here.
- Stress: Tensile versus compressive stress will increase or decrease, respectively, the band gap.[8]
- Mid-gap states or relaxed states, such as sur-

face/interface states, sub-oxide states, defect states and doping[6,9–11] create an alternative path for e-h recombination.

- Nanostructure shape: The shape of a nanostructure can be irregular, which breaks symmetry in the crystal. Thereby, selection rules are broken, the effective mass of the carriers is modified and the overall strength of the confinement is modified.[7]

- Phonon bottleneck: Relaxation via phonons can only occur if the energy difference between the levels is *exactly* matched by the phonon energy.[12] The influence of phonons is discussed further in Sec. II.

- State-filling effects: Under the influence of a large excitation power, higher energy levels will become populated and change the relaxation dynamics.[13]

- Auger processes: This phenomenon has been observed in porous-Si (por-Si).[14]

- Finite confinement potential: Compared to an infinite confinement potential, the finite case will correspond to an overall lowering of the electronic energy levels.[15] Carriers can exhibit tunnelling effects, and/or when a distribution of nanostructure sizes exist[7], super-radiance effects are possible.[16] A discussion of the infinite and finite confinement model is given in Sec. II and IV.

- Temperature: Thermal relaxation has been shown to primarily affect the full width half maximum of the resulting PL spectrum.[17]

Although we do not consider the above effects in our model, they are discussed throughout this article when appropriate. At present, we consider a relatively simple model of direct e-h recombination using a 'particle in a box' type model as a perturbation to the effective mass theory. The advantages of this toy model over others (for example see Refs. 15, 18, and 19) include no adjustable parameters[69] and the transparency of the physics involved. Both factors are very useful for direct comparisons between different systems of confinement.

The model is applied to experimental results on crystalline and amorphous Si and Ge nanostructures, including quantum wells (QWs), wires (Q-wires) and dots (QDs). Si and Ge are considered because due to their elemental nature a few of the factors discussed above can be ignored. Systems of regular shape are chosen to ensure crystallinity is the primary parameter. For example, data obtained by van Buuren et al.[20] for high quality 'star-shaped' samples are difficult to analyse theoretically. In so doing, we are able to get a revealing picture of how the electron and hole behave in the crystalline (c) versus the amorphous (a) system.

Theoretical modelling can be further complicated by the accuracy of nanostructure size determination. Transmission electron microscopy (TEM) is the direct method to determine nanostructure size; however, if the contrast between the matrix and the nano-structure is poor, then the size uncertainty can be on the order of 1 nm.[21] Indirect size determinations can be used as well, such as with x-ray diffraction (XRD)[22] or x-ray photo-emission spectroscopy (XPS).[23] Furthermore, QC in Ge has been a greater challenge for researchers to observe than in Si, because of the tendency to form defects, interfacial mixing and sub-oxide states.[10,24–26] Therefore, only limited results on Ge are discussed here. However, there is recent progress in this area, showing very promising results.[27]

## II. THEORY

In this work, we use the effective mass approximation (EMA). Extensive arguments appear in the literature concerning the validity of the EMA and its $\mathbf{k}\cdot\mathbf{p}$ generalization. On the one hand, it is argued and demonstrated that the EMA overestimates the $E_G$.[7,18] In part, this is because due to QC the parabolic nature of the bands is possibly removed. Another complication can arise from the fact that the envelope functions may not be slowly-varying over the unit cell. However, in this article it is shown that in some cases the EMA can underestimate the $E_G$. Another complication for EMA is in its applicability to a-materials. Street has argued that while it is strictly not justified in the a-system, due to nonspecifically-defined $\mathbf{k}$ vectors, it is still widely used albeit with differing assumptions.[28] We will discuss further the application of the EMA to both amorphous and nano-structured systems in Sec. IV.

On the other hand, it has been argued by Sée et al. that the EMA is well justified.[29] Such arguments reside in the fact that it is not clear what all the relevant parameters are in a nano-structured system of a particular material. In general, the boundary conditions of the system become very important, which is a problem for all theories.[30] If the Fourier components of the envelope function are centred around the the Brillouin zone centre, then envelope functions can be justified. In addition, this justification has been extended to consider that if the interface is defect free then the EMA is justified.[30] Other considered corrections to the EMA use a fourth order term in $\mathbf{k}$.[7] The advantage of the EMA is that it is straightforward in its application, thus allowing one to highlight key features of individual systems. Furthermore, as compared to empirical methods,[31] which produce a dimensional dependence of $D^{-1.39}$, the EMA has the correct units ($D^{-2}$, see (3)).

The Bohr radius of an electron (e), hole (h) or exciton (X) is given by, in SI units:

$$a_{e(h)(X)} = \frac{4\pi\epsilon\hbar^2}{m^*_{e(h)(X)}e^2},$$

$m^*_{e(h)(X)}$ is the effective mass of the e, h or X, respectively, $e$ is the electric charge and $\epsilon$ is the dielectric constant. Depending on the e or h effective mass, the X-Bohr

radius is 4.5 nm for Si and 24 nm for Ge. The Bohr radius defines the spatial dimension of the particles, which determines the range of sizes for which QC can be observed. We define three regimes of confinement here:[7]

- Weak confinement: When the dimension of the system is much larger than $a_e$ and $a_h$. In this situation, the appropriate mass in the kinetic term is $M = m_e^* + m_h^*$. The energy term is dominated by the Coulomb energy.
- Medium confinement: When the dimension of the system is much smaller than $a_e$, but larger than $a_h$, then only electrons will experience confinement. The relevant mass is simply $m_e^*$ for the kinetic term. Most materials belong to this class.
- Strong confinement: When the dimension of the system is much smaller than $a_e$ and $a_h$. Here both electrons and holes experience confinement and the relevant mass is the reduced mass, $\mu$, with $\frac{1}{\mu} = \frac{1}{m_e^*} + \frac{1}{m_h^*}$. In this regime, the Coulomb term is small and can generally be treated as a perturbation.

Below we will use the terms 'weak,' 'medium' and 'strong' to refer to the different regimes of confinement discussed above.

Si and Ge are both indirect gap materials, meaning that, in principle, phonon scattering events are essential to maintain momentum and energy conservation during a radiative event. This situation is true in the case of a bulk material; however, as the dimension of the system is reduced, the uncertainty in the momentum $\mathbf{k}$ vector is increased. Therefore, it is possible to break the $\mathbf{k}$ selection rules making the $E_G$ 'pseudo-direct,' allowing for direct e-h recombination.[32] The length scale at which this 'pseudo-direct' phenomenon becomes important is typically less than a few nanometres.[19,33,34] This length scale corresponds to the systems considered here; therefore, theoretically it is valid to assume direct e-h recombination without phonon-assistance.

In the 'particle in a box' model the bulk $E_G$ is taken as the ground state energy. The effect of reduced dimension is considered as a perturbation to the bulk $E_G$. Therefore, we consider the general field Hamiltonian for a system of Coulombic interacting particles given by (details are given in Ref. 35):

$$\mathcal{H} = \int d^3r \psi^\dagger(r) \left( \frac{-\hbar^2}{2m} \bigtriangledown^2 \right) \psi(r) + \frac{1}{2} \int d^3r d^3\acute{r} \psi^\dagger(r) \psi^\dagger(\acute{r}) \frac{e^2}{4\pi\epsilon|r-\acute{r}|} \psi(\acute{r})\psi(r), \quad (1)$$

where $\psi(r)$ is the field operator, $m$ is the mass of the electron or hole, $\epsilon$ is the dielectric constant of the surrounding medium and $e$ is the electric charge. We do not consider the spin-orbit interaction here, because the fine-structure is beyond the scope of this work.

The field operators are expanded in a two-band model for the conduction band $C$ and the valence band $V$ as:

$$\psi(r) = \sum_k a_{k,i} \varphi_{k,i}(r) \ \ (i \in C, V), \quad (2)$$

where $k$ represents a summation over momentum states. The $\varphi_{k,i}(r)$ basis set in Eq. (2) is expanded to reflect the use of an infinite confinement potential with a Bloch basis $u_{k,i}$. Infinite confinement is a reasonable assumption for the systems we are considering, because the matrix material has a $E_G$ several eV higher than the nano-structure; however, we can not discuss hopping or other such higher order effects. Bloch states reflect the periodic nature of the crystal (Luttinger-Kohn representation), while the boundary conditions of a nanostructure do not reflect this same periodicity. However, in many nanostructures the transitions we are interested in happen near the Brillouin zone centre, e.g. the $\Gamma$-point. This statement may not be strictly true in the case of weak confinement, because $k$-selection rules are not as strongly broken as in the case of strong confinement. Nonetheless, $\mathbf{k} \cdot \mathbf{p}$ perturbation theory considers expansions about the Brillouin zone minimum, $\mathbf{k}_o$. Therefore, we may justify the use of Bloch states through the use of the slowly varying wave approximation whereby only the $\mathbf{k}_o$=0 states are retained.

For indirect gap materials the exciton is Wannier-like, in the limit $k \ll \frac{\pi}{a_c}$ ($a_c$ is the lattice spacing) and we can drop the exchange term, which goes to zero quickly. Equation (1) is solved in the exciton basis using the state $\Phi$ defined as an e-h pair above the ground state, $\Phi_0$, as: $\Phi = \sum_{k_1 k_2} C_{k_1 k_2} a_{k_1}^\dagger b_{k_2}^\dagger \Phi_V$, & $\Phi_V = b_{k_3} b_{k_4} \cdots b_{k_N} \Phi_0$, where $a_k$ ($b_k$) refers to electrons (holes) in the conduction (valence) band. Expanding in low lying $k$-states near the band edge, we solve $E_G(D) = \langle \Phi | \mathcal{H} | \Phi \rangle$, which gives the variation of gap energy with nano-structure size.

For the mass terms in Eq. (1), we use the effective masses calculated using the density of states.[36] The effective mass is related to the parabolicity of the band structure, which is not expected to change in a nanostructure compared to a bulk material at the $\Gamma$-point. Therefore, we assume the effective mass from the bulk system. For Si the effective masses at room temperature are: $m_c \rightarrow m_c^* = 1.08 m_o$ and $m_V \rightarrow m_V^* = 0.57 m_o$. For Ge the effective masses are: $m_c \rightarrow m_c^* = 0.56 m_o$ and $m_V \rightarrow m_V^* = 0.29 m_o$. These definitions yield the equation:

$$E_{Gap}(D) = E_{Gap}(\infty) + \frac{A}{D^2} \, \mathrm{eV} \cdot \mathrm{nm}^2. \quad (3)$$

$E_{Gap}(\infty)$ is the band gap of the bulk material and $D$ represents the QD diameter, the QW thickness or the Q-Wire diameter in what follows. The calculation was carried out for confinement in 1D, 2D with cylindrical coordinates and 3D with spherical coordinates. The parameter $A$ is given for Si and Ge in the strong, medium and weak confinement regimes in Table I. The other fixed parameter is the appropriate $E_G(\infty)$ of the bulk system

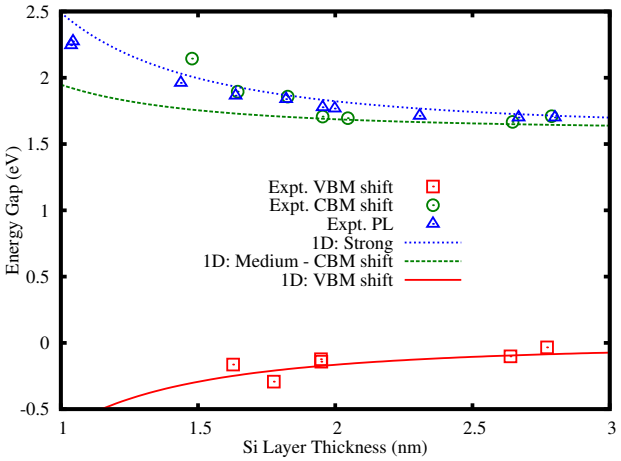


FIG. 1. Disordered Si-QW data and theoretical fit. Experimental data from Ref. 37. Theoretical fit using $A$=0.89 and $E_{Gap}(\infty) = 1.6$ eV in Eq. (3). NB: The CBM shift is offset by the $E_{Gap}(\infty)$.

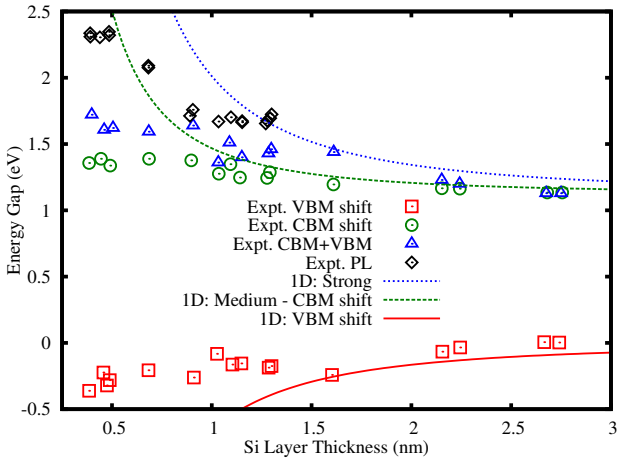


FIG. 2. Crystalline Si-QW data and theoretical fit. Experimental data from Ref. 23. Experimental PL data from Ref. 39. Theoretical fit using $A$=0.35 and $E_{Gap}(\infty) = 1.12$ eV in Eq. (3). NB: The CBM shift is offset by the $E_{Gap}(\infty)$.

and one could argue for the use of a renormalized effective mass with dimension of the system, which is discussed in Sec. IV.

## III. RESULTS

### A. Silicon

#### 1. *Quantum Well*

$Si/SiO_2$ superlattice Si-QWs have been grown using molecular beam epitaxy, determined to be disordered via Raman scattering measurements, and their thickness found using TEM and XRD.[37,38] The change in the VBM and CBM position was measured using XPS and Si $L_{2,3}$ edge absorption spectroscopy, respectively, and room temperature PL spectroscopy was measured. Fig. 1 plots the model predictions with the experimental data; $\Delta E_{CBM}$ is labelled as 'medium confinement,' because a $\Delta E_{CBM}$ is equivalent to QC of the electron only as defined by our model.

In Ref. 37 the authors used a fitting procedure according to the effective mass theory for the $\Delta E_{VBM(CBM)}$, resulting in $\Delta E_{VBM} = -0.5/D^2$ and $\Delta E_{CBM} = 0.7/D^2$, where $D$ is the thickness of the QW. Our model predicts $\Delta E_{VBM} = -0.66/D^2$ and $\Delta E_{CBM} = 0.35/D^2$. The trend for $\Delta E_{CBM}$ is more accurately given in Ref. 37. In Ref. 38, the change in $E_G$ was fitted with $A = 0.7$ and $E_{Gap}(\infty)$=1.6 eV, as in Eq. (3). The fit also determined the effective mass to be $m^*_{h(e)} \approx 1$. The model uses $E_{Gap}(\infty)$=1.6 eV to fit the experimental PL data well when employing the curve for strong confinement with $A = 0.89$.

Next we look at c-$Si/SiO_2$ QWs fabricated by chemical and thermal processing of silicon-on-insulator wafers.[23] The same methods described above were used to determine experimentally the $\Delta E_{VBM(CBM)}$ and the change in the gap energy including the total electron yield for a better signal to noise ratio. The thickness of the Si layer was determined by XPS using a mean free path in Si of $\sim$1.6 nm. Note that a thickness of 0.5 nm corresponds to a single unit cell of Si. Therefore, experimental data below $\approx$ 1 nm should be treated with caution. In a parallel study, these c-$Si/SiO_2$ QWs were investigated optically.[39]

Fig. 2 compares experimental measurements and the model results for c-Si-QWs. The $E_G(\infty)$ in the model is 1.12 eV and the $\Delta E_{VBM}$ is not significant below 1.5 nm. The $\Delta E_{CBM}$, $\Delta E_{CBM+VBM}$, and the experimental PL are all well fitted by the curve for medium confinement, with $A = 0.35$. In Ref. 39 it was found that there is a second PL peak fixed with respect to the Si layer thickness at 1.8 eV. This second peak was associated with interface states. Therefore, we can assign the experimental PL data in Fig. 2 with direct e-h recombination modelled by medium confinement.

#### 2. *QDs*

First we consider Si QDs formed by ion implantation in $SiO_2$ films, followed by high-temperature annealing in $N_2$ and forming gas.[40] Ref. 40 reports the QD diameter and crystalline structure observed by TEM, and room temperature PL measurements. TEM data show a Gaussian distribution in the Si-QD diameter with depth, resulting in a stretched exponential PL dynamic.[4,40]

We compare ion-implanted Si-QDs with Si QDs in a $SiO_2$ matrix prepared by microwave plasma decomposition (MPD) creating ultrafine and densely packed Si QDs[22] (implying that tunnelling effects are important

TABLE I. Parameter $A$ given in Eq. (3) for 3D, 2D and 1D confinement.

| | 3D | | | 2D | | | 1D | | |
|---|---|---|---|---|---|---|---|---|---|
| | Strong | Medium | Weak | Strong | Medium | Weak | Strong | Medium | Weak |
| Si | 3.57 | 1.39 | 0.91 | 2.09 | 0.81 | 0.53 | 0.89 | 0.35 | 0.23 |
| Ge | 7.88 | 2.69 | 1.77 | 4.62 | 1.58 | 1.04 | 1.97 | 0.67 | 0.44 |

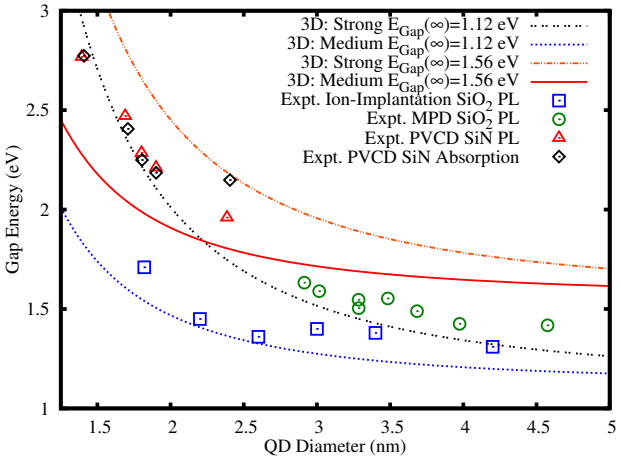


FIG. 3. Crystalline and amorphous Si-QD data and theoretical fit. 'Expt. Ion-Implantion $SiO_2$' refers to crystalline Si QDs embedded in $SiO_2$ from Ref. 40. 'Expt. microwave plasma decomposition (MPD) $SiO_2$' refers to crystalline Si QDs embedded in $SiO_2$ from Ref. 22. 'Expt. plasma enhanced chemical vapour deposition (PCVD) SiN' refers to amorphous Si QDs embedded in SiN from Ref. 43. Theoretical fit using $A$=3.57 and 1.39 and $E_{Gap}(\infty)$ = 1.12 or 1.56 eV (as labeled) in Eq. (3). NB: The absorption data is offset by the $E_{Gap}(\infty)$.

here[41]). The crystallinity and size was determined by TEM imaging and XRD, respectively. In Ref. 22, the authors note that PL was not observed unless the Si QDs were oxidized, implying that surface bonds were passivated with suboxide states eventually forming a surround $SiO_2$ matrix.

Fig. 3 shows the experimental PL data for ion-implantated and MPD Si QDs together with our calculated curves for strong and medium confinement. Above 3 nm both sets of experimental data follow closely the model of strong confinement with $A$=3.57 and $E_G(\infty)$=1.12 eV. This indicates that for sample diameters larger than this size tunnelling effects are significant, implying a de-localization of carrier states. Iacona et al. measured a similar trend for experimental PL data.[42] Below 3 nm, when QC effects are particularly strong, the ion-implantation data follows the curve for medium confinement, with $A$=1.39.

Next we consider a-Si QDs embedded in a SiN matrix.[43] The Si QDs were fabricated using plasma enhanced chemical vapour deposition. The size and amorphous structure were measured using TEM and the PL was taken at room temperature. Absorption data was taken by ultraviolet-visible absorption spectroscopy. The value for the bulk band gap given by the authors is 1.56 eV, which is obtained via a fitting procedure. This value is known to vary between 1.5→1.6 eV, for Si samples prepared similarly.[43]

We can see in Fig. 3 that the experimental data for absorption and PL of a-Si QDs embedded in SiN lies between the curve for medium ($A$=1.39) and strong ($A$=3.57) confinement, with $E_{Gap}(\infty)$=1.56. Using a fitting procedure, the authors of Ref. 43 found $A$=2.40. The authors further conclude that by observing the fact that the experimental absorption data lies close to the PL data, one can conclude that the PL data for these samples is a good measure of the actual change in the $E_G(D)$.[43] Notice that this situation is similar to that observed for Si-QWs (see Fig. 1 and 2).

### 3. *Quantum Wires*

Due to inherent complications in the fabrication process of Si or Ge wires with a diameter below the Bohr radius, few studies on QC in nano-wires exist and we are only able to report on c-Si-Q-wires. On the other hand, por-Si studies are widely cited in the literature. With suitable control of the etchant, por-Si QDs can become elongated,[44] thus breaking confinement in one direction implying they are more wire-like; a detailed discussion is provided in Ref. 45. In this case, they are called pseudo-por-Si-QDs or in the case they behave like interconnected dots, spherites.[46]

Anodically grown por-Si samples were prepared by Schuppler et al.[47] X-ray absorption measurements determined the structures to be closer to c-Si than to a-Si. TEM was used to determine the size and PL measurements were performed at room temperature. The por-Si structures are said to be H-passivated and O-free; however, samples were exposed to air.

Si Q-wires were produced by Ma et al. using an oxide-assisted growth method with SiO powders.[48] Subsequently, the wires were cleaned with HF to remove the oxide, thus forming a H-terminated surface. Scanning tunnelling microscopy was used to determine the diameter of the wires. The formation of $SiH_2$ and $SiH_3$ was observed on the facets of the Q-wires, which was attributed to bending stresses in the wires. The energy gap was determined using scanning tunnelling spectroscopy, which also indicated doping levels in the wires as seen by an

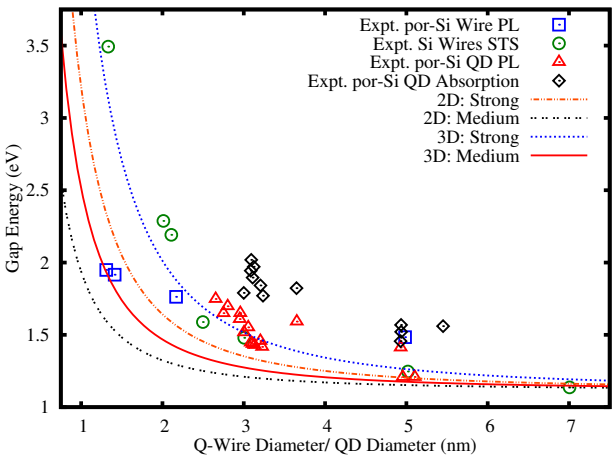


FIG. 4. Crystalline Si Q-wire and QD data and theoretical fit. Experimental por-Si wire data from Ref. 47. Experimental Si Wire data from Ref. 48, using scanning tunnelling spectroscopy (STS). Experimental por-Si QD data from Ref. 46 and 50. Theoretical fit using $A$=1.39 and 0.81 and $E_{Gap}(\infty) = 1.12$ eV in Eq. (3). NB: The absorption data is offset by the $E_{Gap}(\infty)$. NB: 'QD' here refers to spheroids.

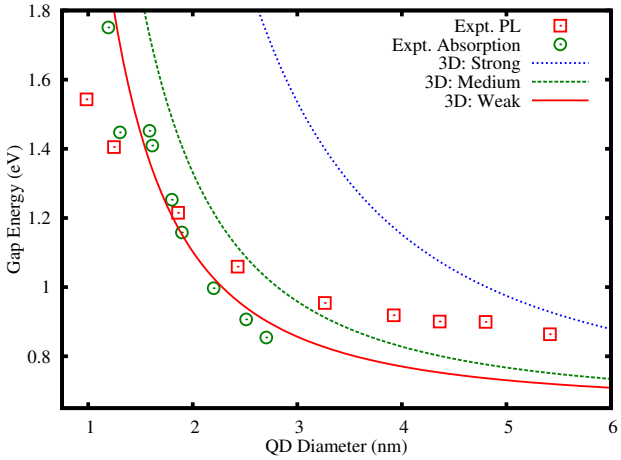


FIG. 5. Crystalline Ge-QD data and theoretical fit. Experimental Ge QDs data from Ref. 51. Experimental Ge absorption data from Ref. 52. Theoretical fit using $A$=2.69 and $E_{Gap}(\infty) = 0.66$ eV in Eq. (3).

asymmetrical shift of the $E_G$ around 0 V.

The experimental data from Ma et al. and Schuppler et al. can be seen in Fig. 4. Below 3 nm the experimental data from Schuppler et al. ('por-Si Wire PL') lie close to the curve for 2D strong confinement with $A$=2.09 and $E_{Gap}(\infty)$=1.12 eV. Notice that the experimental data also lie close to the curve for 3D medium confinement with $A$=1.39. This observation may be a reflection of the idea that these structures are between dots and wires. On the other hand, the data from Ma et al. lie close to the curve for 3D strong confinement, using the same $E_{Gap}(\infty)$ and $A$=3.57. We also note that recently Si-Q-wires have been produced[49] with results nearly identical to those of Ma et al.

Experimental data on pseudo-por-Si-QDs for both absorption and PL are taken from Ref. 46 and 50. Raman and TEM measurements were used to determine the size and the 'spherite' nature of the samples, respectively. PL measurements were performed at room temperature and at 4.2K, with very little difference in the two measurements. Optical absorption was performed at room temperature. It is also noted in Ref. 50 that, for por-Si, interface states and phonon events are significant. Fig. 4 shows the PL and absorption experimental data for por-Si-QDs. Here the experimental data are modelled by the curve for 3D strong confinement, with $A$=3.57 and the same gap energy as above. Compared to absorption and PL data for a-Si-QDs in Fig. 3 and the Si-QWs in Fig. 1 and 2, there is a significant shift between the absorption data and the PL data, indicating a Stokes shift in the emission.[50] Furthermore, as noted in Ref. 46, the experimental PL data are nearly identical to Takagi et al., shown in Fig. 3.

### B. Germanium

The first observation of QC in Ge was by Takeok et al.[51] In this study, they produced Ge QDs using an rf co-sputtering method followed by thermal annealing. The size of the Ge QDs was controlled by varying the initial Ge concentration and was later determined by TEM imaging, which also showed that the Ge QDs were highly crystalline. PL was performed at room temperature.

In a more recent study, Ge QDs were produced by condensation out of the gas phase onto a Si substrate cleaned by HF.[52] The Ge QDs were determined to be in the bulk diamond crystalline phase. X-ray absorption (XAS) data were taken and can be seen in Fig. 5. XAS excites the Ge 2p electron into the conduction band; therefore, the researchers obtained data for the change in the conduction band.

The experimental data from Refs. 51 and 52 are presented in Fig. 5. Note that the absorption data are obtained by shifting the Bostedt et. al. data by the $E_G(\infty)$ of Ge at 0.66 eV. Further note that above 3 nm there is a nearly identical departure from the medium confinement curve into strong confinement as was seen with Si-QDs in Fig. 3. In general, both sets of experimental data are well modelled by the curve for medium confinement with $A$=2.69 and $E_{Gap}(\infty) = 0.66$ eV. For the smaller sizes (below 2.5 nm) the behaviour appears to deviate from medium confinement. This result may be because for the smaller sizes the authors only estimated the sizes.[51] In Ref. 52 the size was determined using atomic force microscopy, which is known to improperly determine the width of an object.[53] Therefore, if the QDs are not symmetric then the diameter measurements could be inaccurate.

## IV. DISCUSSION

To summarize the comparisons made in Sec. III, we first consider the relationship between experimental absorption and PL data. In the case of disordered-Si-QWs (Fig. 1), c-Si-QWs (Fig. 2) and a-Si-QDs in SiN (Fig. 3) the absorption curve follows closely with the PL. As mentioned in Sec. III A 2, this result indicates that the PL measurement is an accurate measure of $E_G(D)$. Furthermore, in the case of Si-QWs the VBM does not change significantly. Therefore, we conclude that the model dependence between these three systems does not lie in the change in the VBM.

Considering the absorption data from por-Si-QDs (Fig. 4), there is a significant shift between the absorption data and PL data, which was noted in Sec. III A 3. In addition, the por-Si QD data are nearly identical to the MPD Si-QDs (Fig. 3), which indicates that these systems are structurally similar with similar decay dynamics. In the case of por-Si it has been found that this system is under tensile stress.[54] Tensile stress, which is a function of the thickness of oxide, is known to increase the band gap.[55] It is known that the surrounding oxide has a strong effect on the resulting PL in por-Si.[56] The resulting Si-O-Si bonds due to the oxidation process place large stresses on the por-Si crystallites. In addition, it has been shown that the dominant PL comes from surface states.[50] At the surface or interface states, it has been shown that band bending on the order of 0.2→0.3 eV can occur.[57] Such a shift in energy corresponds with the discrepancy shown in Fig. 3 and 4.

For the c-Si-Q-wires measured by STS (Fig. 4), the data are modelled by strong confinement. This is because of the stresses observed in the system and possibly because of the doping; both are factors that do change the nature of electronic structure. In Sec. III A 3, we mentioned that these structures experience bending stress, which has a tensile component. Furthermore, Fig. 4 illustrates that c-Si-Q-wires are identical in energy to por-Si; therefore, the analysis of these systems is similar. By contrast, the por-Si wire PL data (Fig. 4) behaves more wire-like, which may be a result of the fact the authors took care to minimize oxygen exposure (see Sec. III A 3).

From Fig. 3 and 5, both ion implanted Si-QDs and Ge-QDs have the same behaviour above 3 nm. They lie close to the curve for strong confinement, similar to the case of por-Si, indicating that possible stresses or interface states are important in this regime. Ge is known to experience stress in a $SiO_2$ matrix.[58] Tensile stress can be relieved depending on the nature of the interface bonds and the surface to volume ratio of Si:$SiO_2$.[55] In the work of Ref. 35 it was found from Raman spectroscopy that ion-implanted QDs are not under stress for diameters smaller than 3 nm. Therefore, c-Si-QDs produced by ion implantation and c-Ge-QDs are well modelled by medium confinement below 3 nm.

Finally, a-Si-QDs in SiN (Fig. 3) lie between medium and strong confinement (see Sec. III A 2). SiN has a band gap of 5.3 eV versus $SiO_2$ at 9.2 eV, which allows for tunnelling of carrier states.[43] More importantly, if we consider the nucleation process during thermal annealing and consider the bond enthalpies for diatomic species (SiN at 470 kJ/mol and SiO at 799 kJ/mol), it is easier to break SiN bonds, thus allowing for a greater degree of intermixing at the QD-matrix interface. Therefore, a SiN matrix acts more like a finite potential barrier, which lowers the gap energy from the infinite case. A numerical computation indicates that the difference between the case of finite versus infinite confinement potential is between 10% and 15% depending on the size of the system. This difference exactly corresponds with the difference we see in Fig. 3. Therefore, we conclude that a-Si-QDs in SiN are well modelled by strong confinement.

From the results above and considering modifications that must be made to our model to account for non-direct e-h recombination phenomena, it is clear that strong confinement describes a-materials and medium confinement describes c-materials. Therefore, since QC of a particle is a function of the delocalization of that particle with respect to the dimension of the system, we need to account for the fact that the hole becomes more delocalized in the a-system than in the c-system. This fact may or may not be seen as a shift in the VBM. As noted above, disordered-Si-QWs, c-Si-QWs and a-Si-QDs in SiN all do not show a large variation in the VBM.

A mechanism for pinning of the hole states in c-Si-QDs was discussed in the work of Sa'ar et al. as a function of the hole coupling with vibrons.[59] However, this phenomenon does not account for the fact that the hole becomes more delocalized in the a-system, it is well known that band-tail states play a very important role in the band structure of a-materials, even though the population density is relatively low.[28] Kanemitsu et al. (and Refs. within), report the experimental observation that the band-tail states become strongly delocalized in the a-system, while the hole remains relatively localized in the c-system.[60] This observation accounts for what is observed in this work.

Another critical factor to discuss is the effective mass concept, particularly in the a-system. Recall from Sec. II, the bulk effective mass is used in the calculations. It is possible that this parameter is not well-justified in the a-system[28] and is simply not valid in the nanostructured system, in the worst possible case, or it is size-dependent.[61–63]

The a-system has typically 80%[64] of the density of the c-system, while disordered Si generally refers to a density $\approx 98\%$[65] of that of c-Si, and these values can vary widely based on the preparation method.[66] Therefore, short and medium range structural order does remain in both of these systems. Although the long-range order is not well-defined in the a-system along with the **k**-vectors, alternative approaches to this concept have been extensively presented. In an earlier work, Kivelson et al. defined an alternative approach to this concept.[67] They formulated the assumptions (i) the structure of the solid can

be approximated by a rigid continuous random network that is homogeneous on the scale of the slowly varying envelope, and (ii) the band can be measured by a set of linearly independent orbits, which are not necessarily orthogonal. Furthermore, Kivelson et al. used a tight-binding approach with approximate eigenvalues to obtain the effective mass Hamiltonian. In another approach[68], Singh looked at the effective masses in the extended and tail-states around the mobility edge directly using a real-space formulation. The electron energy eigenvalues are given in terms of the probability amplitude, which cannot be defined as in the case of a c-material in terms of **k**-vectors. Instead, the probability amplitude is defined as[68]:

$$C_{1l} = N^{-1/2} \exp(i\mathbf{s}_e \cdot \mathbf{l}), \text{ with } \mathbf{s}_e(E) = \sqrt{\frac{2m_e^*(E - E_C)}{\hbar^2}}$$

where $E_C$ defines the mobility edge; therefore, the effective mass is defined above the mobility edge in the extended states and is imaginary in the tail states. In either approach described here, the result is that the effective mass calculated is lower than in the bulk system.

The size dependence of the effective mass in c-systems is reported in Refs. 61–63. Experimentally, the effective mass is reported to decrease with size in Ref. 62 and 63. In one theoretical report, the hole effective mass increases, while the electron effective mass decreases.[61] The magnitude of change in the effective mass is roughly the same for the electron and the hole, and considering the effective mass of the electron in the bulk system is roughly twice that of the hole, it is not likely that the change will be within experimental resolution. Overall, the effective mass in the a-system and in the nano-structured system is understood to decrease, but the magnitude of the decrease is unclear. Therefore, in terms of the calculations presented here, if the effective mass is lowered than we should expect to see an increase on the calculated $E_G$ and hence our curves will shift upwards. However, we would also expect to see an increase in $E_G$ from the experimental results because a lowering of the effective mass means an increase in the Bohr radius and hence stronger confinement effects should be observed. Since the exact magnitude of these changes is not known it is difficult to evaluate the error incurred by using the bulk effective mass.

## V. CONCLUSION

We have studied the effect of confinement dimensions and crystallinity on the magnitude of the band gap expansion (as a function of decreasing size) in group IV semiconductor nanostructures (quantum wells (QWs), wires (Q-wires) and dots (QDs). Medium and strong confinement models provide the best fit to experimental results; moreover crystalline materials exhibit medium confinement, while amorphous materials exhibit strong confinement regardless of the confinement dimensions of the system. This difference in confinement strength was explained by considering the extent of spatial delocalization of the hole. A possible explanation is hole pinning due to coupling with the vibronic states.[59] It has previously been reported[60] that band tail states become strongly delocalized in the amorphous system compared to the crystalline system. This hole delocalization would partially account for the trends observed in our work. The concept of the effective mass was reviewed for the amorphous system. We argue that the effective mass can still be defined in the amorphous material around the mobility edge.[67,68] A lower value of the effective mass is reported for the amorphous system, while the hole mass increases and the electron mass decreases as a function of spatial confinement.[61–63] With the diminished effective mass (the absolute value of this change is not possible to estimate, and more work is needed in this area), we expect an increase in $E_{Gap}$, and our calculated curves of energy versus diameter will be shifted upwards. However the general trends observed in this work will remain the same.

* ebarbagi@uwo.ca


[1] W. R. Frensley and H. Kroemer, Phys. Rev. B. **16**, 2642 (1977)

[2] editorial, Nature Nanotechnology **5**, 381 (2010)

[3] H. Haken, *Quantum field theory of solids* (North-Holland Pub. Co., Amsterdam, 1976)

[4] J. Linnros, N. Lalic, A. Galeckas, and V. Grivickas, J. Appl. Phys. **86**, 6128 (1999)

[5] *Quantum Dots: a Doorway to Nanoscale Physics*, edited by W. D. Heiss (Springer, Berlin, 2005)

[6] D. J. Lockwood and L. Pavesi, "Silicon photonics," in *Topics in Applied Physics*, Vol. 94, edited by D. J. Lockwood and L. Pavesi (Springer, Berlin, 2004) pp. 1–52

[7] A. D. Yoffe, Advances in Physics **51**, 799 (2002)

[8] G. L. Bir and G. E. Pikus, *Symmetry and Strain-Induced Effects in Semiconductors* (Wiley, New York, 1976)

[9] G. Hadjisavvas and P. C. Kelires, Phys. Rev. Lett. **93**, 226104 (2004)

[10] E. Barbagiovanni, S. Dedyulin, P. Simpson, and L. Goncharova, Nuc. Instr. and Meth. in Phys. Res. B, doi:10.1016/j.nimb.2011.01.036(2011)

[11] S. Godefroo, M. Hayne, M. Jivanescu, A. Stesmans, M. Zacharias, O. I. Lebedev, G. V. Tendeloo, and V. V. Moshchalkov, Nature Nanotechnology **3**, 174 (2008)

[12] A. Valentin, J. Sée, S. Galdin-Retailleau, and P. Dollfus, J. Phys.: Conf. Ser. **92**, 012048 (2007)

[13] L. V. Dao, X. Wen, M. T. T. Do, P. Hannaford, E. C. Cho, Y. H. Cho, and Y. Huang, J. Appl. Phys. **97**, 013501 (2005)

[14] D. Kovalev, H. Heckler, M. Ben-Chorin, G. Polisski, M. Schwartzkopff, and F. Koch, J. Porous Mater. **7**, 85 (2000)
[15] D. B. Tran Thoai, Y. Z. Hu, and S. W. Koch, Phys. Rev. B. **42**, 11261 (1990)
[16] R. H. Dicke, Phys. Rev. **93**, 99 (1954)
[17] T. Orii, M. Hirasawa, T. Seto, N. Aya, and S. Onari, Eur. Phys. J. D. **24**, 119 (2003)
[18] A. Zunger, Phys. Stat. Sol. (b) **224**, 727 (2001)
[19] N. Tit, Z. H. Yamani, J. Graham, and A. Ayesh, Mater. Chem. Phys. **24**, 927 (2010)
[20] T. van Buuren, L. N. Dinh, L. L. Chase, W. J. Siekhaus, and L. J. Terminello, Phys. Rev. Lett. **80**, 3803 (1998)
[21] B. Garrido, M. López, A. Pérez-Rodríguez, C. García, P. Pellegrino, R. Ferrè, J. A. Moreno, J. R. Morante, C. Bonafos, M. Carrada, A. Claverie, J. de la Torre, and A. Souifi, Nuc. Instr. and Meth. in Phys. Res. B **216**, 213 (2004)
[22] H. Takagi, H. Ogawa, Y. Yamazaki, A. Ishizaki, and T. Nakagiri, Appl. Phys. Lett. **56**, 2379 (1990)
[23] Z. H. Lu and D. Grozea, Appl. Phys. Lett. **80**, 255 (2002)
[24] Q. Wang, F. Lu, D. Gong, X. Chen, J. Wang, H. Sun, and X. Wang, Phys. Rev. B. **50**, 18226 (1994)
[25] G. Jin, Y. S. Tang, J. L. Liu, and K. L. Wang, Appl. Phys. Lett. **74**, 2471 (1999)
[26] K. S. Min, K. V. Shcheglov, C. M. Yang, H. A. Atwater, M. L. Brongersma, and A. Polman, Appl. Phys. Lett. **68**, 2511 (1996)
[27] N. L. Rowell, D. J. Lockwood, I. Berbezier, P. D. Szkutnik, and A. Ronda, J. Electrochem. Soc. **156**, H913 (2009)
[28] R. A. Street, *Hydrogenated Amorphous Silicon* (Cambridge University Press, Cambridge, 1991)
[29] J. Sée, P. Dollfus, and S. Galdin, Phys. Rev. B. **66**, 193307 (2002)
[30] B. Lassen, R. V. N. Melnik, and M. Willatzen, Commun. Comput. Phys. **6**, 699 (2009)
[31] C. Delerue, G. Allan, and M. Lannoo, Phys. Rev. B. **48**, 11024 (1993)
[32] D. Kovalev, H. Heckler, M. Ben-Chorin, G. Polisski, M. Schwartzkopff, and F. Koch, Phys. Rev. Lett. **81**, 2803 (1998)
[33] M. S. Hybertsen, Phys. Rev. Lett. **72**, 1514 (1994)
[34] T. Takagahara and K. Takeda, Phys. Rev. B. **46**, 15578 (1992)
[35] E. G. Barbagiovanni, L. V. Goncharova, and P. J. Simpson, Phys. Rev. B. **83**, 035112 (2011)
[36] P. Y. Yu and M. Cardona, *Fundamentals of Semiconductors: Physical and Material Properties (3rd ed.)* (Springer, Berlin, 2001)
[37] Z. H. Lu, D. J. Lockwood, and J. M. Baribeau, Nature **378**, 258 (1995)
[38] D. J. Lockwood, Z. H. Lu, and J. M. Baribeau, Phys. Rev. Lett. **76**, 539 (1996)
[39] D. J. Lockwood, M. W. C. Dharma-wardana, Z. H. Lu, D. H. Grozea, P. Carrier, and L. J. Lewis, Mater. Res. Soc. Symp. Proc. **737**, F1.1.1 (2003)
[40] C. R. Mokry, P. J. Simpson, and A. P. Knights, J. Appl. Phys. **105**, 114301.1 (2009)
[41] B. V. Kamenev, G. F. Grom, D. J. Lockwood, J. P. McCafrey, B. Laikhtman, and L. Tsybeskov, Phys. Rev. B. **69**, 235306 (2004)
[42] F. Iacona, G. Franzo, and C. Spinella, J. Appl. Phys. **87**, 1295 (2000)
[43] N. M. Park, C. J. Choi, T. Y. Seong, and S. J. Park, Phys. Rev. Lett. **86**, 1355 (2001)
[44] H. S. Seo, X. Li, H. D. Um, B. Yoo, J. H. K. K. P. Kim, Y. W. Cho, and J. H. Lee, Mater. Lett. **63**, 2567 (2009)
[45] B. Hamilton, Semicond. Sci. Technol. **10**, 1187 (1995)
[46] D. J. Lockwood and A. G. Wang, Solid State Commun. **94**, 905 (1995)
[47] S. Schuppler, S. L. Friedman, M. A. Marcus, D. L. Adler, Y.-H. Xie, F. M. Ross, T. D. Harris, W. L. Brown, Y. J. Chabal, L. E. Brus, and P. H. Citrin, Phys. Rev. Lett. **72**, 2648 (1994)
[48] D. D. D. Ma, C. S. Lee, F. C. K. Au, S. Y. Tong, and S. T. Lee, Science **299**, 1874 (2003)
[49] H. Yoshioka, N. Morioka, J. Suda, and T. Kimoto, J. Appl. Phys. **109**, 064312 (2011)
[50] D. J. Lockwood, Solid State Commun. **92**, 101 (1994)
[51] S. Takeoka, M. Fujii, S. Hayashi, and K. Yamamoto, Phys. Rev. B. **58**, 7921 (1998)
[52] C. Bostedt, T. van Buuren, T. M. Willey, N. Franco, L. J. Terminello, C. Heske, and T. Möller, Appl. Phys. Lett. **84**, 4056 (2004)
[53] P. Eaton and P. West, *Atomic Force Microscopy* (Oxford University Press, Oxford, 2010) p. 110
[54] L. Z. Kun, K. Y. Lan, C. Hao, H. Ming, and Q. Yu, Chin. Phys. Lett. **22**, 984 (2005)
[55] C. C. Hong, W. J. Liao, and J. G. Hwu, Appl. Phys. Lett. **82**, 3916 (2003)
[56] M. V. Wolkin, J. Jorne, P. M. Fauchet, G. Allan, and C. Delerue, Phys. Rev. Lett. **82**, 197 (1999)
[57] S. V. Svechnikov, E. B. Kaganovich, and E. G. Manoilov, Semi. Phy. Quantum Elect. Optoelect. **1**, 13 (1998)
[58] I. D. Sharp, D. O. Yi, Q. Xu, C. Y. Liao, J. W. Beeman, Z. Liliental-Weber, K. M. Yu, D. N. Zakharov, J. W. Ager, D. C. Chrzan, and E. E. Haller, Appl. Phys. Lett. **86**, 063107 (2005)
[59] A. Sa'ar, Y. Reichman, M. Dovrat, D. Krapf, J. Jedrzejewski, and I. Balberg, Nano Lett. **5**, 2443 (2005)
[60] Y. Kanemitsu, J. Luminescence **100**, 209 (2002)
[61] K. Seino and F. Bechstedt, Semicond. Sci. Technol. **26**, 014024 (2011)
[62] B. Rößner, G. Isella, and H. von Känel, Appl. Phys. Lett. **82**, 754 (2003)
[63] Z. Yang, Y. Shi, J. Liu, B. Yan, R. Zhang, Y. Zheng, and K. Wang, Mater. Lett. **58**, 3765 (2004)
[64] L. Ley, "The physics of hydrogenated amorphous silicon ii," in *Topics in Applied Physics*, Vol. 56, edited by J. D. Joannopoulos and G. Lucovsky (Springer, New York, 1984) p. 61
[65] Z. H. Lu, D. J. Lockwood, and J. M. Baribeau, Solid State Electronics **40**, 197 (1996)
[66] O. Renmer and J. Zemek, Czech. J. Phys. B **23**, 1273 (1973)
[67] S. Kivelson and C. D. Gelatt, Phys. Rev. B. **19**, 5160 (1979)
[68] J. Singh, J. Non-Cryst. Solids **299**, 444 (2002)
[69] The effective mass can be taken as an adjustable parameter, which is not done in this work. The exact value of the effective mass is not known for nanostructures, see Sec. IV.